J. Fluid Mech. (1976), *vol.* 77, *part* 1, *pp.* 81–103
Printed in Great Britain

Higher eigenstates in boundary-layer stability theory

By D. CORNER, D. J. R. HOUSTON AND M. A. S. ROSS

Physics Department, University of Edinburgh, Scotland

(Received 16 August 1974 and in revised form 28 April 1976)

Using the Orr–Sommerfeld equation with the wavenumber as the eigenvalue, a search for higher eigenstates in the stability theory of the Blasius boundary layer has revealed the existence of a number of viscous states in addition to the long established fundamental state. The viscous states are discrete, belong to two series, and are all heavily damped in space. Within the limits of the investigation the number of viscous states existing in the layer increases as the Reynolds number and the angular frequency of the perturbation increase. It is suggested that the viscous eigenstates may be responsible for the excitation of some boundary-layer disturbances by disturbances in the free stream.

1. Introduction

The Orr–Sommerfeld equation is a fourth-order linear and homogeneous ordinary differential equation with linear and homogeneous boundary conditions, and therefore has an eigenvalue solution. It represents the conditions governing a periodic wave of very small amplitude travelling downstream in a two-dimensional incompressible parallel flow, and gives the distribution of wave amplitude in the direction transverse to the mean flow. If the boundaries of the flow in the transverse direction are a finite distance apart, one might reasonably expect to find an infinite series of *discrete* eigenvalues. If, however, one boundary lies at infinity, one might expect to find a *continuous* spectrum of eigenvalues. The Orr–Sommerfeld equation is used for flows that take place between parallel walls a finite distance apart, but it is also used for the flat-plate boundary layer (in the parallel-flow approximation), where the lower boundary is the flat plate and the upper boundary is taken at infinity. This 'infinity' is a necessary mathematical assumption required for the calculation of both the mean flow in the layer and its perturbation, but the physical thickness of the layer is effectively finite, limited in definable ways for a real fluid at a finite Reynolds number. The physical limitation on thickness enters the Orr–Sommerfeld equation through the functions of the mean flow which occur in the coefficients of the dependent variable and its second derivative. In the boundary-layer case the existence of one *discrete* eigenvalue is well known, and the question then arises whether other discrete values exist.

The equation contains three parameters; the Reynolds number R of the mean flow and two parameters characteristic of the perturbing wave: either α, the wavenumber, and c, the wave velocity, or α and the angular frequency $\beta\,(=\alpha c)$.

R and one of the wave parameters are given arbitrary real positive values, and the remaining parameter becomes the eigenvalue, in general a complex quantity. In all the early studies of the Orr–Sommerfeld equation, c was taken as the eigenvalue. If the imaginary part of c is positive the wave is amplified in time. The existence of multiple eigenvalues means that there are many values of c for one choice of R and α and, in the absence of degeneracy, each eigenvalue can exist only if its own eigenfunction is excited.

In an analytical study of the eigenvalues of the Orr–Sommerfeld equation, Morawetz (1952) discussed three cases: (i) plane Couette flow, (ii) plane Poiseuille flow and (iii) the flat-plate boundary layer in the parallel-flow approximation. The analysis was based on Lin's (1944) second form of solution (using asymptotic series). Two kinds of eigenvalue were shown to exist. The first kind consisted of eigenvalues each of which in the limit of vanishing viscosity (or infinite Reynolds number) approached asymptotically an eigenvalue of the Rayleigh inviscid equation for the case concerned. Eigenvalues of this kind were finite in number (and thus discrete) in a bounded region of the c plane, and they existed only in cases 2 and 3. The second kind of eigenvalue was discrete and characteristic only of the viscous equation. Such eigenvalues were found in cases 1 and 2 but not in case 3. For a given value of α and sufficiently large R, a finite number of values of the second kind existed within a bounded region of the c plane, but as R and the domain of c increased, the number of these values increased without limit. In case 2, one root c of each of the following equations existed for each value of n:

$$\operatorname{Im}\int_{z_1}^{z_2}[i(U-c)]^{\frac{1}{2}}\,dz = \begin{cases} n\pi/\lambda, \\ (n+\frac{1}{2})\,\pi/\lambda, \end{cases}$$

where $\lambda = (\alpha R)^{\frac{1}{3}}$ and the flow extends from z_1 to z_2.

In a later study of cases 1 and 2, Schensted (1961) derived the eigenvalues of the second kind by a different method. She exploited her method to show not only that the number of eigenvalues was denumerably infinite when $|i\alpha cR|$ increased indefinitely but also that the corresponding eigenfunctions formed a complete set. Any arbitrary transverse distribution of the perturbation stream function $f(z)$ could therefore be expressed as an infinite series in the eigenfunctions $\phi_n(z)$:

$$f(z) = \sum_{n=1}^{\infty} a_n \phi_n(z). \tag{1}$$

The coefficients a_n could be determined by applying the orthogonality relation:

$$\int_{z_1}^{z_2} \phi_n (D^2-\alpha^2)\,\chi_m\,dz = \int_{z_1}^{z_2} \chi_m (D^2-\alpha^2)\,\phi_n\,dz = \delta_{mn},$$

where $\phi_n(z)$ and $\chi_m(z)$ are normalized eigenfunctions representing respectively the solutions of the Orr–Sommerfeld equation and the adjoint equation when the boundary conditions and arbitrary parameters are the same for both equations and the flow extends from z_1 to z_2. Schensted discussed the application of (1) to initial-value problems, to forced vibration problems and to nonlinear stability theory. In the last of these applications it was shown that the nonlinear terms (which cease to be negligible for larger amplitudes of the perturbation) have two

physical influences: (i) nonlinear effects produced by a single eigenstate and (ii) nonlinear coupling between pairs of eigenstates. Interest in nonlinear processes as precursors of the onset of turbulence has led to many developments of nonlinear stability theory during the past 25 years.

There is one aspect of boundary-layer stability which has been found particularly difficult to discuss theoretically, namely the coupling between the free stream and the boundary layer which allows disturbances in the free stream to be taken up in the boundary layer. The level of free-stream turbulence has been shown by various authors, but notably by Schubauer & Klebanoff (1955), to influence the onset of turbulence in boundary layers. This is a problem that has no counterpart in other applications of the Orr–Sommerfeld equation. Mathematically, the outer boundary conditions are applied at infinity. Physically, the outer limit lies where the downstream component of mean velocity reaches the free-stream value; beyond this limit the flow is assumed to be inviscid for a physically infinite distance. This model is adequate for the study of boundary-layer properties when the external flow in not independently perturbed, but it is not a suitable model for the direct analysis of the coupling between the external flow and the boundary layer when the external flow is the source of a perturbation. Boundary conditions which are compatible with the accepted equations for the motion cannot easily be formulated for transmission of disturbances through 'infinity' from the inviscid to the viscous region. If eigenstates of the Orr–Sommerfeld equation could be shown to exist which possess fluctuations in the inviscid region, and if they could be superposed on the well-known fundamental eigenstate and then interact with it, a method of attack on the coupling problem might be developed.

The present investigation has been carried out to discover whether the boundary-layer stability equation has multiple eigenstates when the perturbation has a purely real frequency. A preliminary study of this kind has been published by Jordinson (1971). He solved the Orr–Sommerfeld equation numerically, and found a number of values of c for both time-amplified and space-amplified conditions. In the present work a similar numerical method is used, but the solution is found only for space-amplification conditions. The corresponding time-amplification problem has recently been studied by Mack (1976).

2. The numerical method

A rectangular co-ordinate system is used, with the y axis coincident with the leading edge of the flat plate and the z axis normal to the surface of the plate. The free-stream velocity U_0 (in the x direction) and the displacement thickness of the layer δ_1 are used as units of velocity and length, and the Reynolds number is then $R = U_0\delta_1/\nu = m^2x$, where m is the Blasius constant $\sim 1{\cdot}7208$. The mean flow in the boundary layer is represented non-dimensionally by $U(z)$, the downstream component of the total Blasius flow. The perturbation is represented non-dimensionally by the stream function

$$\psi(x, z; t) = \phi(z)\, e^{i(\alpha x - \beta t)}. \tag{2}$$

Substitution of (2) in the linearized vorticity equation gives the Orr–Sommerfeld equation in space-amplification form:

$$[(D^2-\alpha^2)^2-iR(\alpha U-\beta)(D^2-\alpha^2)+i\alpha RU'']\phi = 0, \tag{3}$$

where $D = d/dz$, $U'' = d^2U/dz^2$, β and R are known real positive parameters, and α is the complex eigenvalue (with positive real part).

The boundary conditions for (3) express the fact that the perturbation vanishes at $z = 0$ and as $z \to \infty$; at the outer limit we also have $U = 1$ and $U'' = 0$. At the plate surface we have

$$\phi(0) = D\phi(0) = 0. \tag{4a}$$

As z approaches infinity, (3) becomes

$$[(D^2-\alpha^2)^2-iR(\alpha-\beta)(D^2-\alpha^2)]\phi = 0, \tag{4b}$$

which has four solutions of the form e^{kz}, where k is $\pm\alpha$ or $\pm\gamma$, and γ is the root with positive real part of

$$\gamma^2 = \alpha^2+iR(\alpha-\beta).$$

Only two of the values of k are compatible with the outer conditions, and as $z \to \infty$ we have

$$\phi = Ae^{-\alpha z}+Be^{-\gamma z}. \tag{4c}$$

Since there are two conditions to be satisfied at the outer limit, the two constants A and B can be determined.

In the well-known solution of (3) and (4), $\alpha_r \ll \gamma_r$, and the outer boundary condition is sufficiently accurately given by writing $B = 0$, but this simplification is possible only when $\arg\gamma$ does not rise to nearly $\frac{1}{2}\pi$. To examine the situation when $\alpha_r-\beta$ falls to zero, with $R = O(10^3)$ and both α_r and α_i of order unity γ may be expressed in the form

$$\gamma = i(\alpha_i R)^{\frac{1}{2}}\left[1-\frac{\alpha_r^2-\alpha_i^2}{\alpha_i R}-i\left(\frac{2\alpha_r\alpha_i}{\alpha_i R}+\frac{\alpha_r-\beta}{\alpha_i}\right)\right]^{\frac{1}{2}}.$$

When $\alpha_r-\beta = 0$, binomial expansion gives a convergent series for γ, the highest-order terms for γ_r and γ_i being respectively $\alpha_r(\alpha_i/R)^{\frac{1}{2}}$ and $(\alpha_i R)^{\frac{1}{2}}$. Then

$$0 < \gamma_r \ll \alpha_r$$

and the γ term in (4c) is the important one for eigenvalue determination. When γ_r falls to zero, (4c) no longer satisfies the outer boundary condition, but this does not occur until $\alpha_r-\beta = -2\alpha_r\alpha_i R^{-1}$, and valid solutions are possible above this limit. The residual errors in the numerical solution will contribute an uncertainty to the determination of the lower limit for α_r; this uncertainty reaches its maximum in the part of the α plane around $\alpha_r-\beta = 0$, where the weighting of α_r to α_i in γ^2 is about $O(\alpha)/O(R)$.

The solution of (3) and (4) is found by a finite-difference method described in detail by Ross & Corner (1972). The method includes transformation of $\phi(z)$ into a closely related function $g(z)$ to improve the accuracy of the finite-difference approximation during the integration stage. The finite-difference equations, incorporating the boundary conditions, are then given by

$$\mathbf{M}(\alpha)\,\mathbf{g} = 0. \tag{5}$$

where $\mathbf{M}(\alpha)$ is an $n \times n$ pentadiagonal matrix with complex elements and $\mathbf{g}$ is a vector with n complex components. If a good approximation to α is known the solution to (5) is obtained by an iterative method which gives results correct to h^4, where h is the net spacing. The numerical results are valid only when this convergence rate is attained. A sufficiently accurate result is usually obtained with 80 net points covering the range of integration $0 \leqslant z \leqslant 6$. For higher accuracy, a smaller net spacing is used, and in some cases an extended range of z.

If a good approximation to α is not known, or if a number of unknown eigenvalues is sought, we use the fact that, for a non-trivial solution of (5) to exist, $\det \mathbf{M}(\alpha) = 0$. The non-zero elements of $\mathbf{M}(\alpha)$ are, with four exceptions, constants or polynomials in α with constant coefficients; the exceptional elements have exponents of $-h\alpha$, $-2h\alpha$, $-h\gamma$ and $-2h\gamma$ as coefficients. The function $\det \mathbf{M}(\alpha)$ therefore has no poles when α and R remain finite, but since γ is double-valued when unrestricted, $\det M(\alpha)$ has two branch points given by $\gamma = 0$. One of these lies in the first quadrant of the α plane at

$$\alpha = \left(\beta - \frac{2\beta^3}{R^2} + \ldots\right) + i\left(\frac{\beta^2}{R} - \frac{5\beta^4}{R^3} + \ldots\right),$$

and the second lies in the third quadrant. The locus of $\gamma_r = 0$ in the α plane is the hyperbola

$$\alpha_r = \frac{R}{R + 2\alpha_i}\beta.$$

The area searched was limited to $\alpha_r \geqslant \beta$, $\alpha_i \geqslant 0$, lying on one side of this line. The number of zeros of $\det \mathbf{M}(\alpha)$ within a suitable contour C is

$$N = \frac{1}{2\pi}\int_C d[\arg \det \mathbf{M}(\alpha)].$$

Rectangular contours were used, and systematic subdivision of the area of C allowed each zero to be located to the accuracy required for an iterative solution.

After higher eigenstates had been found by the method described above, it was possible to trace the changes in their eigenvalues for constant forcing frequency $F\,(= \beta/R)$ and varying R by extrapolation, using the relation

$$\left(\frac{\partial\alpha}{\partial R}\right)_F = \left(\frac{\partial\alpha}{\partial R}\right)_\beta + F\left(\frac{\partial\alpha}{\partial\beta}\right)_R,$$

followed by iterative solution. When $\arg\gamma$ changes continuously this process can give values of α such that $\gamma_r < 0$. Eigenvalues of this kind will be referred to here as 'non-physical'. The use of an extrapolation technique to pass from the physical to the non-physical solution makes it easy to ensure that Wasow's (1948) monoticity condition is satisfied.

3. The extended form of the Orr–Sommerfeld equation

The 'parallel mean flow approximation' used in deriving (3) assumes that all x derivatives of the mean flow stream function $\overline{\psi}$ are negligible. If, instead, we neglect only second- and higher-order x derivatives of $\overline{\psi}$, and take

$$W = -\partial\overline{\psi}/\partial x,$$

the accuracy of the mean flow representation becomes the same as that of the Prandtl boundary-layer equation (Barry & Ross 1970). In place of (3) we then have the extended equation

$$[(D^2-\alpha^2)^2-iR(\alpha U-\beta-iWD)(D^2-\alpha^2)+i\alpha RU''+RW''D]\phi = 0. \quad (6)$$

The boundary conditions for ϕ are unchanged at $z = 0$, but in place of (4*b*) we have

$$[(D^2-\alpha^2)^2-iR(\alpha-\beta-iW_\infty D)(D^2-\alpha^2)]\phi = 0,$$

and the solution of this equation is, for $z\to\infty$,

$$\phi = Ae^{-\alpha z}+Be^{-\mu z}, \quad (7)$$

where

$$\mu = [\gamma^2+(\tfrac{1}{2}RW_\infty)^2]^{\frac{1}{2}}-\tfrac{1}{2}RW_\infty, \quad (7a)$$

In our conditions $|\gamma^2|$ is greater than $(\frac{1}{2}RW_\infty)^2$ by a large factor, and the important difference between (7) and (4*c*) arises from the last term in (7*a*). The real part of μ must still be positive; there is a small region of the Riemann surface for α where $\gamma_r > 0$ but $\mu_r < 0$, and eigenvalues of (6) occurring in this region will be non-physical. A few solutions of (6), (4*a*) and (7) were obtained for comparison with the main results.

4. The higher eigenvalues and eigenvectors

Results were initially found for a range of Reynolds numbers and a single non-dimensional frequency, $F = \beta/R = 80\times10^{-6}$, representing a constant physical frequency in an experiment. The first search of the α plane for eigenvalues of (3) and (4) was made at $R = 1000$ and $\beta = 0{\cdot}08$, and the results are shown as points on the α plane in figure 1(*a*). Using $n = 80$ net points ($h = 0{\cdot}075$), the search gave 12 points, marked '$\times$', lying on a slightly curved line near $\alpha_r = \beta$. In order to apply the h^4-convergence test, the numerical integration was repeated with $n = 120$, marked '$\bigcirc$', and $n = 160$, marked '+'. The eigenvalues on the curved line varied almost linearly with h, and thus did not satisfy the h^4 test. It was concluded that these points were eigenvalues of the three matrices, but not of the differential equation. Two other eigenvalues lying to the right of the curved line of points showed very small variations with h which satisfied the h^4 test. It was concluded that these two points were eigenvalues of the differential equation.

The same procedure was carried out using (6), (4*a*) and (7), with the results shown in figure 1(*b*). The area of the α plane that yields non-physical solutions lies to the left of the dashed line $\mu_r = 0$. The curved line of points now lies in the non-physical region, and the points on this line again move to the left as n increases. One stable point showing h^4 convergence lies to the right of the dashed line. Near $\alpha = 0{\cdot}09+0{\cdot}083i$, however, a '$\times$' and '+' indicate the movement of an eigenvalue to the right as n increases, and these points may represent the second stable state found in figure 1(*a*) but now incompletely resolved from points on the curved line.

A similar search over a larger area of the α plane, $\beta \leqslant \alpha_r \leqslant 0{\cdot}6$, $0 \leqslant \alpha_i \leqslant 1$, was

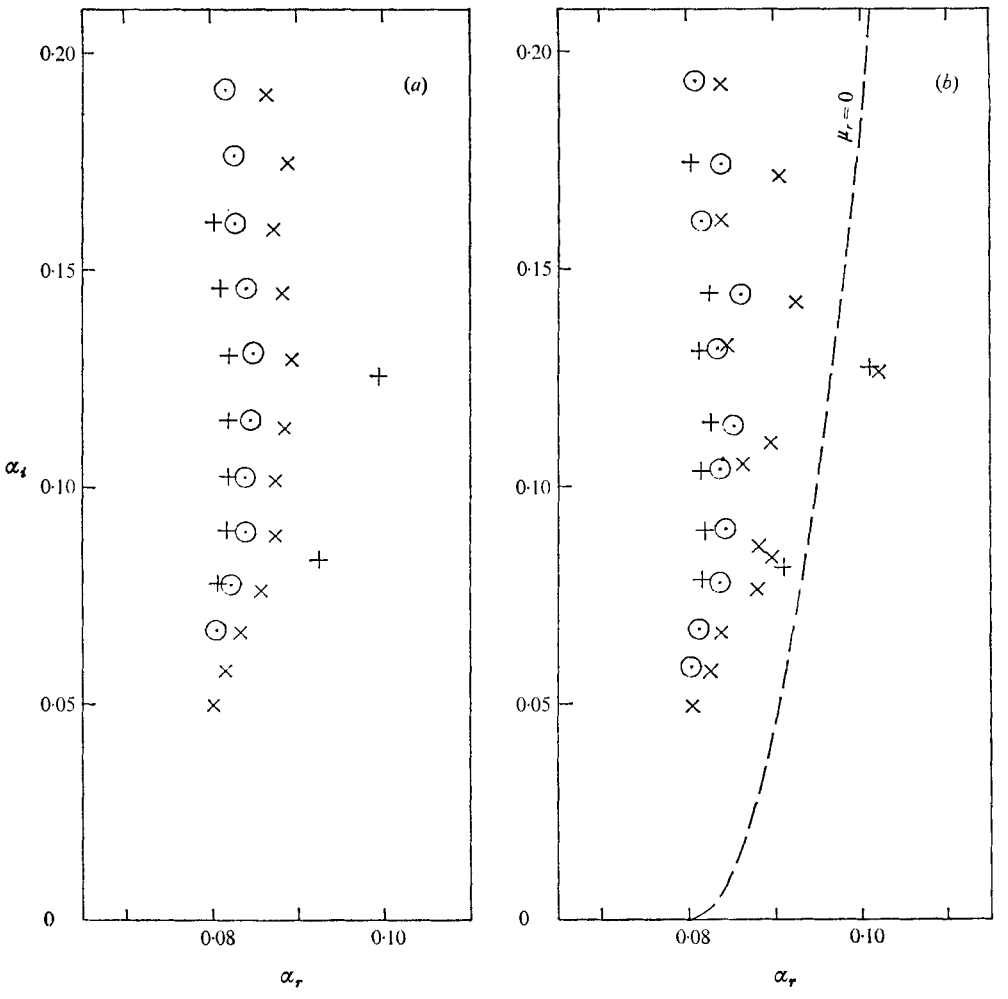

FIGURE 1. Eigenvalues (*a*) of the Orr–Sommerfeld equation and (*b*) of the extended equation for $R = 1000$, $\beta = 0{\cdot}08$. ×, $n = 80$, $h = 0{\cdot}075$; ⊙, $n = 120$, $h = 0{\cdot}05$; +, $n = 160$, $h = 0{\cdot}025$.

made at $R = 1500$ and $\beta = 0{\cdot}12$, using (3) and (4). The results shown in figure 2 were obtained with $n = 80$. In this case the fundamental eigenstate is slightly damped, and its eigenvalue appears close to the α_r axis near $\alpha_r = 0{\cdot}34$. Within the searched area no eigenvalues were found to have a higher value of α_r than the fundamental. When higher values of n were used, the fundamental eigenvalue and the points $\alpha \sim 0{\cdot}24 + 0{\cdot}145i$ and $\alpha \sim 0{\cdot}164 + 0{\cdot}28i$ showed h^4 convergence, but the other points in the figure did not do so. Those lying on the nearly vertical curve showed variations roughly proportional to h. A second line of 6 points appears to split off from the first line, and the value of α_i for these points was found to be inversely proportional to h^2, and they also were rejected.

The two new eigenvalues attributed to the differential equation were followed at constant F and varying R by the extrapolation method and subsequent

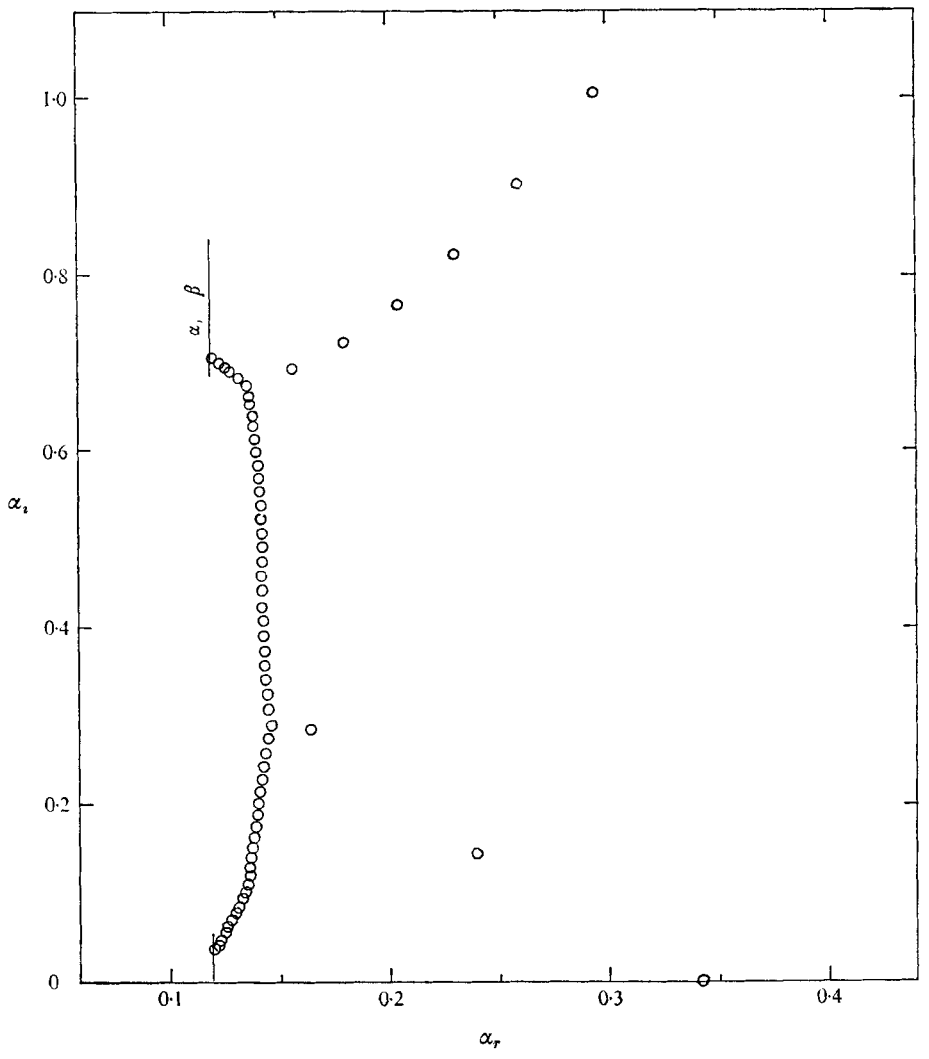

FIGURE 2. Eigenvalues of the Orr–Sommerfeld equation for $R = 1500$, $\beta = 0{\cdot}12$. $n = 80$, $h = 0{\cdot}075$.

iterative solution. The results for $1000 < R < 1500$ are given in table 1. The fact that this process worked well was taken as confirmation of the view that higher eigenvalues of the Orr–Sommerfeld equation had been found.† Regarding the fundamental eigenstate as state 1, we took the new eigenvalues to belong to states 2 and 3, with state 2 having a higher value of α_r than state 3. A graph of α_r, α_i and β *vs.* R is shown for state 2 in figure 3, and a graph of the wave velocities $c_r = \beta\alpha_r/|\alpha|^2$ is shown for states 2 and 3 in figure 4.

† Further confirmation of this conclusion has been provided by L. M. Mack (private communication), who has completed a search by a different numerical method (Mack 1976) for space-amplification eigenvalues at $R = 1500$ and $\beta = 0{\cdot}12$, in the area $\beta < \alpha_r < 0{\cdot}9$, $0 \leqslant \alpha_i < 0{\cdot}62$. He found only the fundamental and two higher eigenvalues, and his values agree with ours to within 0·2%.

Reynolds number	State 2		State 3	
	α_r	α_i	α_r	α_i
1000	0·092690	0·083280	0·099548	0·125715
1050	0·104640	0·090556	0·104671	0·138349
1100	0·117338	0·097334	0·109709	0·151357
1150	0·130528	0·103799	0·115416	0·165916
1200	0·144196	0·110071	0·121137	0·180790
1250	0·158382	0·116210	0·127868	0·196830
1300	0·173146	0·122243	0·134399	0·213854
1350	0·188553	0·128172	0·141036	0·231163
1400	0·204672	0·133989	0·148271	0·248927
1450	0·221580	0·139681	0·155957	0·267450
1500	0·239369	0·145235	0·163965	0·286661

TABLE 1. Eigenvalues at $F = 80 \times 10^{-6}$, standard form of equation

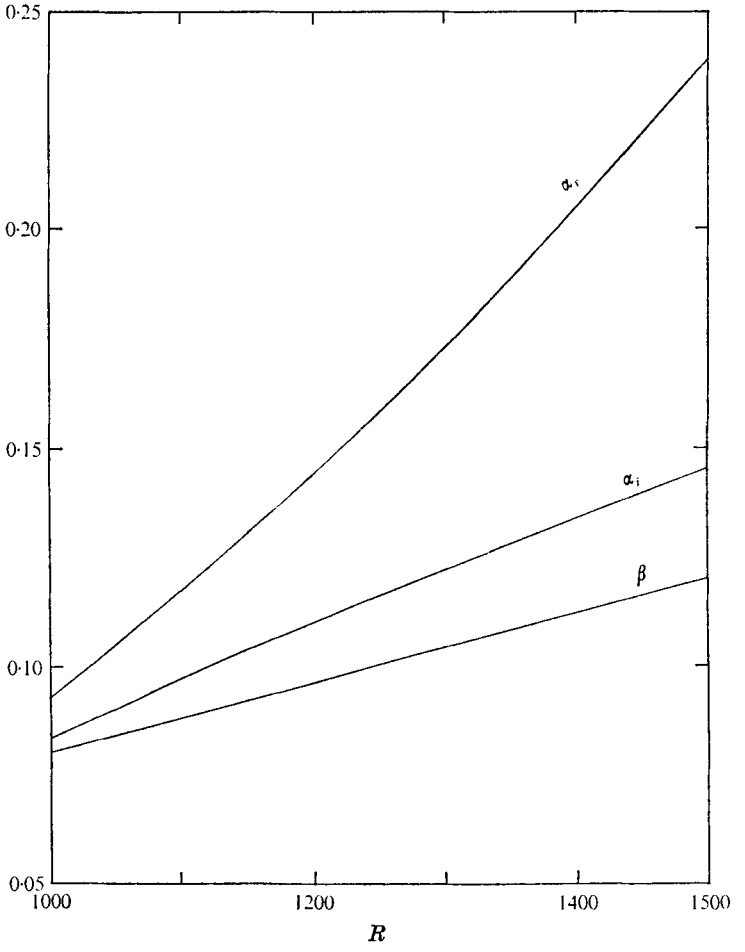

FIGURE 3. Wave parameters α_r, α_i and β *vs.* R for state 2 of the Orr–Sommerfeld equation with $F = \beta/R = 0{\cdot}00008$.

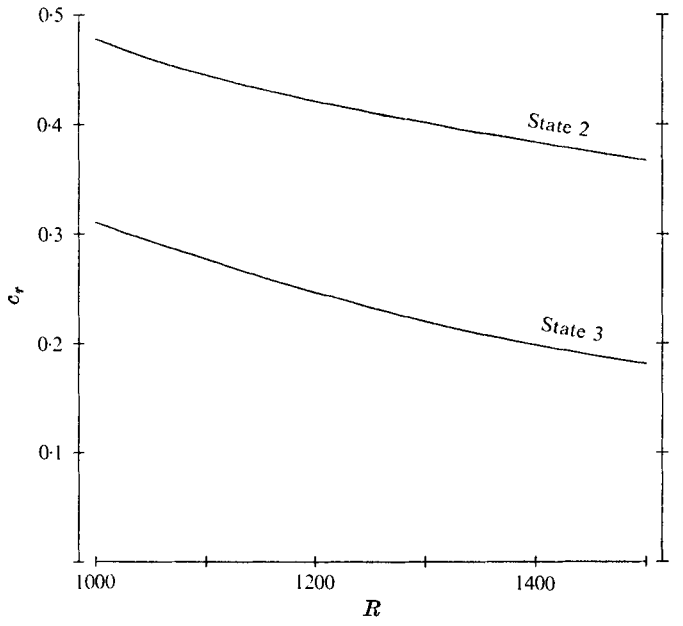

FIGURE 4. c_r *vs.* R for states 2 and 3 of the Orr–Sommerfeld equation.

The functions ϕ_r, ϕ_i, ϕ_r' and ϕ_i' for the Orr–Sommerfeld equation with $F = 80 \times 10^{-6}$ are given for state 2 at $R = 1000$, 1250 and 1500 in figures 5(*a*) (*b*) and (*c*) respectively and for state 3 at $R = 1000$ in figure 5(*d*). The eigenvector functions for state 3 at constant F vary with R in the same manner as those of state 2, i.e. as R decreases the oscillations of $|\phi'|$ extend progressively through a greater depth of the mathematical boundary layer, and become significant far beyond the outer limit of the physical boundary layer. When the eigenvalue passes into the non-physical region the eigenvector has oscillations that grow exponentially in amplitude with increasing z. At $F = 80 \times 10^{-6}$ and $R = 1500$, the eigenvectors for states 2 and 3 of the extended equations show only slight differences from those of the Orr–Sommerfeld equation, but as R is decreased the eigenvectors for the extended equations enter the non-physical region at higher values of R.

It is clear from table 1 and figure 3 that, when F remains constant and R decreases, the values of α_r decrease quite rapidly, the rate of change being more marked for state 2 than for state 3. The eigenvalues of state 2 were therefore followed by the extrapolation method to lower values of R to find out whether α_r would fall below the value of β at some fairly well defined value of R. The curves in figure 6, for values of n of 80, 120 and 160, show that α_r continues to decrease as R decreases, and becomes strongly step-length dependent. The most accurate of the three solutions shows an intersection of the α_r and β lines near $R = 915$, and this value of R is regarded as a lower limit for the excitation of state 2 at the value of F concerned. The curves for α_i in figure 6 show that, when the eigenvalues are (as described in §2 above) not strongly controlled by the differential equation, the matrix imposes a discretization.

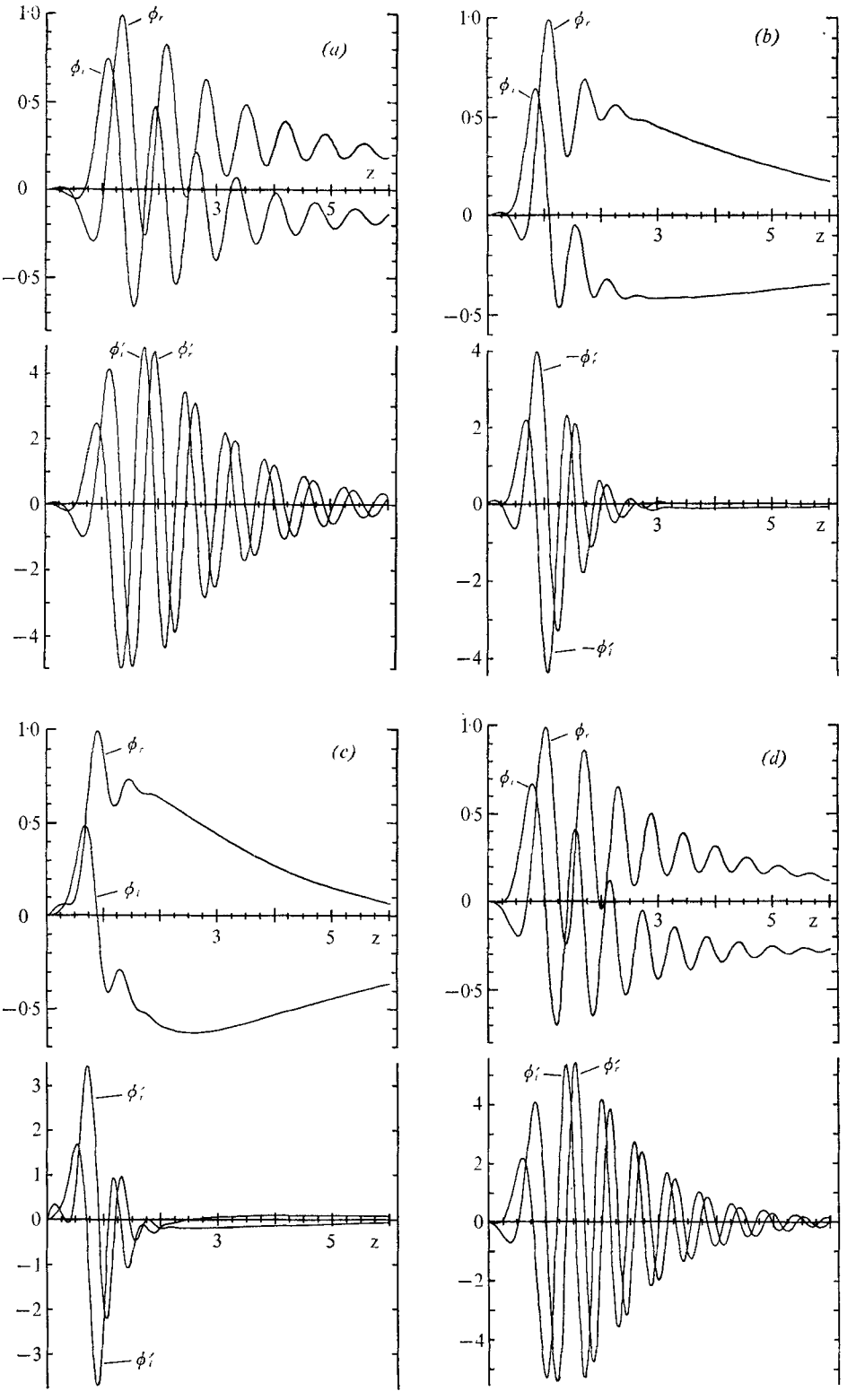

FIGURE 5. The functions $\phi_r(z)$, $\phi_i(z)$, $\phi_i'(z)$ and $\phi_r'(z)$ of the Orr–Sommerfeld equation. (*a*) State 2; $R = 1000$, $\beta = 0{\cdot}08$. (*b*) State 2; $R = 1250$, $\beta = 0{\cdot}10$. (*c*) State 2; $R = 1500$, $\beta = 0{\cdot}12$. (*d*) State 3; $R = 1000$, $\beta = 0{\cdot}08$.

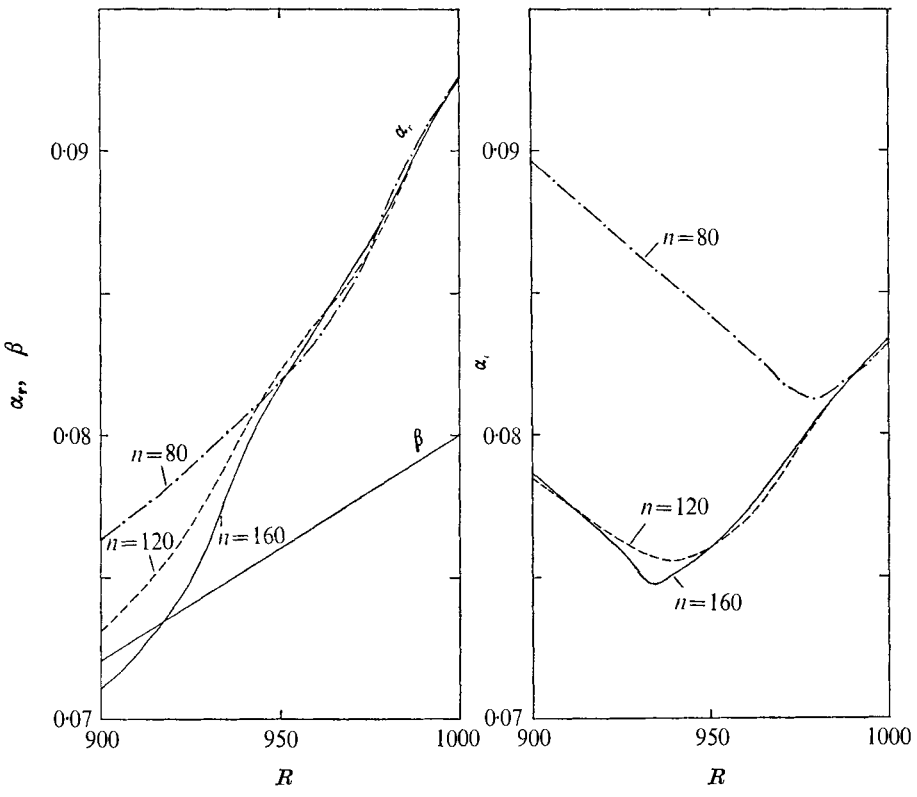

FIGURE 6. Wave parameters α_r, α_i and β *vs.* R for state 2 of the Orr–Sommerfeld equation; a continuation of figure 3 to lower R, using $n = 80$, $n = 120$ and $n = 160$.

The search for higher eigenvalues was continued at $R = 3000$ and $R = 5000$, and the dependence on F was examined. As R and F were increased, more eigenvalues of the differential equation emerged from the line of points. The results obtained at $R = 3000$ are shown in table 2. The increase in R and the recurring problem of separating the emerging eigenvalues from the line of points called for higher resolution. The results in table 2 were obtained with $n = 240$, $0 \leqslant z \leqslant 6$ ($h = 0{\cdot}025$); all the tabulated values satisfied the h^4-convergence test but those shown in brackets were not clearly separated from the line of matrix eigenvalues. The higher states of even order have $\alpha_r > \alpha_i$, and those of odd order have $\alpha_r < \alpha_i$. When F is well above its threshold the eigenvalues occur in pairs, with

$$\alpha_r^{(2n)} \sim \alpha_i^{(2n+1)} \quad \text{and} \quad \alpha_i^{(2n)} \sim \alpha_r^{(2n+1)}.$$

Figure 7 is a graph of $\log \alpha_i$ *vs.* $\log \alpha_r$ for four values of F, the data being taken from table 2. For a given value of F, the points (indicated by an open symbol) lie on two lines, the upper and lower lines being formed respectively by the odd-order and even-order eigenvalues. The straight lines on the graph are drawn through the points for states 3 and 5 and through the points for states 2 and 4. The two lines for one value of F intersect near the point (β, β) (indicated by the corresponding solid symbol), with $\beta = FR$. The distances along any of these

	State 2		State 3		State 4		State 5		State 6		State 7		
10^6F	α_r	α_i	α_r	α_i	α_r	α_i	α_r	α_i	α_r	α_i	α_r	α_i	10^6F
5			0·0195	0·0213									5
10			0·0459	0·0556									10
15	0·0695	0·0590	0·0689	0·0970									15
20	0·1137	0·0827	0·0912	0·1473									20
25	0·1651	0·1043	0·1161	0·2050									25
30	0·2249	0·1240	0·1436	0·2689	(0·1027	0·0876)	(0·1033	0·0989)					30
35					0·1290	0·1091	(0·1217	0·1194)					35
40	0·3822	0·1685	0·2072	0·4132	0·1605	0·1303	(0·1435	0·1676)					40
45					0·1941	0·1523	(0·1613	0·1955)					45
50	0·5648	0·2468	0·2820	0·5779	0·2300	0·1751	0·1908	0·2446					50
55					0·2684	0·1989	0·2081	0·2707					55
60	0·7562	0·3399	0·3685	0·7610	0·3093	0·2238	0·2445	0·3250					60
70	0·9599	0·4442	0·4672	0·9606	0·3985	0·2777	0·3034	0·4122					70
80	1·1760	0·5594	0·5783	1·1747	0·4963	0·3387	0·3675	0·5056	0·3055	0·2439			80
90	1·4040	0·6859	0·7019	1·4015	0·6005	0·4073	0·4367	0·6048	0·3678	0·2893			90
100	1·6428	0·8238	0·8377	1·6398	0·7092	0·4824	0·5109	0·7094	0·4346	0·3377			100
110	1·8919	0·9734	0·9856	1·8885	0·8218	0·5635	0·5900	0·8190	0·5056	0·3898			110
120	2·1501	1·1347	1·1465	2·1465	0·9381	0·6495	0·6741	0·9332	0·5803	0·4456	(0·476	0·576)	120
130	2·4168	1·3080	1·3177	2·4130	1·0581	0·7402	0·7631	1·0517	0·6581	0·5053	0·5367	0·6518	130
140	2·6909	1·4934	1·5022	2·6871	1·1816	0·8355	0·8567	1·1742	0·7385	0·5686	0·5999	0·7211	140
150	2·9718	1·6910	1·6991	2·9679	1·3086	0·9353	0·9551	1·3004	0·8211	0·6353	0·6659	0·8099	150
160	3·2584	1·9010	1·9086	3·2546	1·4387	1·0395	1·0580	1·4300	0·9057	0·7050	0·7349	0·8928	160

TABLE 2. Higher eigenvalues of the Orr–Sommerfeld equation for $R = 3000$

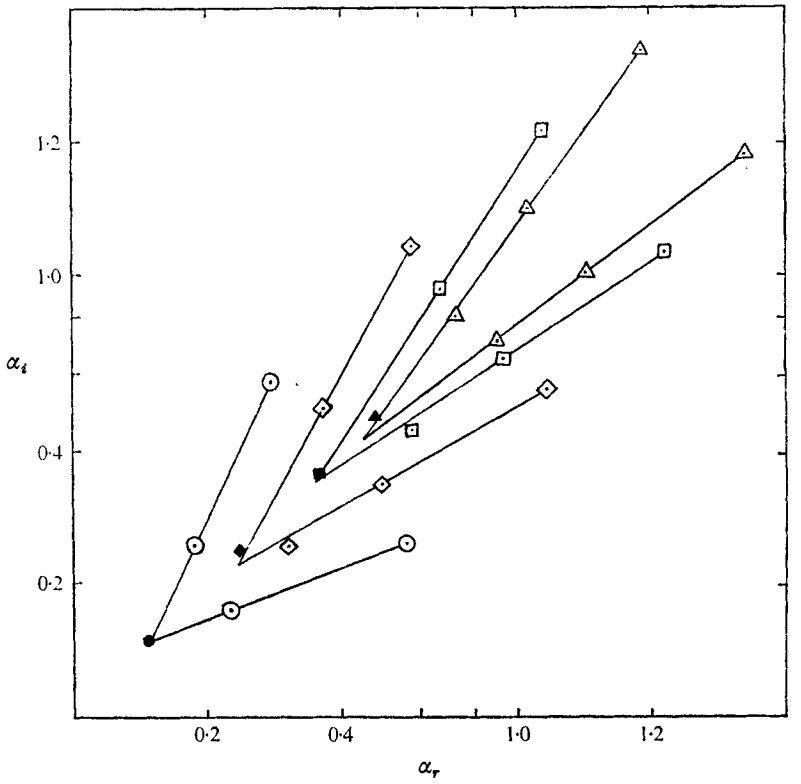

FIGURE 7. Logarithmic plot of α_i *vs.* α_r for all states existing at $R = 3000$. ⊙, $10^6F = 50$; ◇, $10^6F = 80$; ⊡, $10^6F = 120$; △, $10^6F = 160$. Solid symbols represent (β, β) with $\beta = FR$.

lines between the points for states 2 and 4 and between the points for states 3 and 5 are nearly constant. A similar relation exists for states 2 and 6 and states 3 and 7.

5. Interpretation of the results

The nature of the higher eigenstates

At $R = 1000$ the functions ϕ_r' and ϕ_i' for states 2 and 3 show many fluctuations, and in this respect differ greatly from the function $|\phi'|$ for the fundamental eigenstate, which shows only one phase reversal in the range $0 < z < \infty$. All the other higher eigenstates have well-developed oscillatory functions when they emerge from the line of points. The 'mean wavelength' and the 'mean logarithmic decrement per wavelength' were therefore estimated from the differentiated functions in figures 5(*a*) and (*d*) and compared with the corresponding quantities given by e^{-qz}, where $q = [iR(\alpha-\beta)]^{\frac{1}{2}} = q_r + iq_i$. This function was taken as a first approximation to the exponential factor in the asymptotic viscous solution to the Orr–Sommerfeld equation for a boundary layer (Lin 1944):

$$\phi_3(z) = (U-c)^{-\frac{5}{4}} \exp\left\{-\int_{z_c}^{z} [i\alpha R(U-c)]^{\frac{1}{2}}\, dz\right\}. \tag{8}$$

	'Mean wavelength'		'Mean logarithmic decrement'	
	$2\pi/q_i$	Matrix solution	$2\pi q_r/q_i$	Matrix solution
State 2	0·687	0·70	0·482	0·461
State 3	0·560	0·58	0·491	0·486

TABLE 3. Comparison of e^{-qz} with the matrix solution for $\phi'(z)$ for states 2 and 3 at $R = 1000$ and $z > 2$

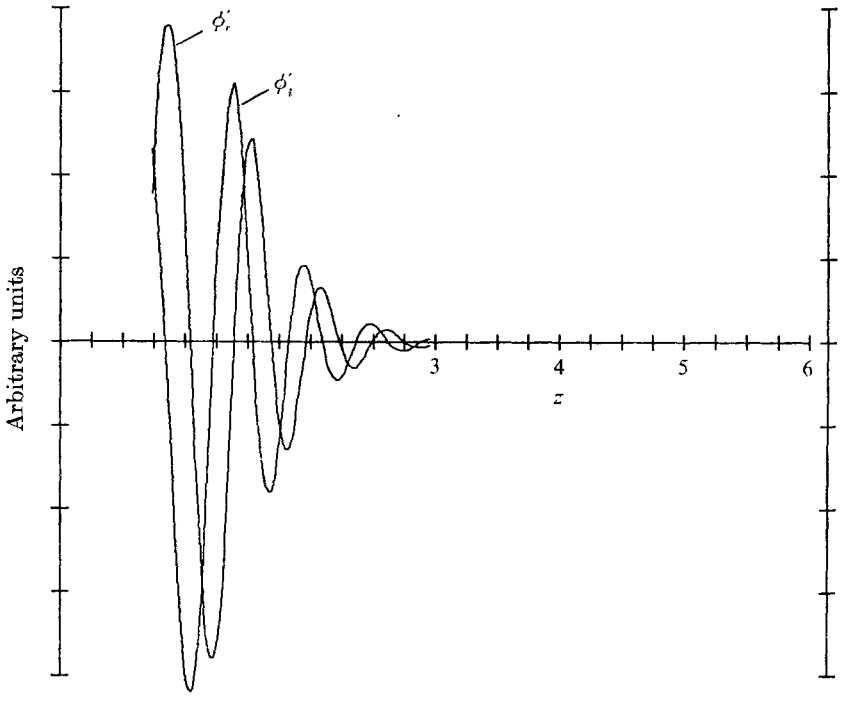

FIGURE 8. Functions $\phi_r'(z)$ and $\phi_i'(z)$ calculated from (9) with the parameters of the functions in figure 5(*b*).

In (8), z is a complex variable and $U(z_c) = c$, but when z is real and greater than 2 the difference between q and the integrand in (8) is negligible for present purposes. The calculated mean wavelength is $2\pi/q_i$ and the calculated decrement is $2\pi q_r/q_i$. These calculated quantities are compared in table 3 with the corresponding properties of the functions ϕ_r' and ϕ_i' in figures 5(*a*) and (*d*). The agreement shown in the table suggests that the eigenfunctions are viscous solutions of (3). At $R > 1000$ and $10^6F = 80$, the logarithmic decrements for state 2 become too large to allow the same test to be applied. A first approximation to ϕ_r' and ϕ_i' was therefore computed from

$$\phi'(z) = -[i\alpha R(U-c)]^{\frac{1}{2}}\,\phi(z), \tag{9}$$

where $\phi(z)$ is given by (8). Figure 8 shows the result of the calculation for $R = 1250$, $\beta = 0{\cdot}10$ and $\alpha = 0{\cdot}1584 + i0{\cdot}1162$. The exponential factor in (8)

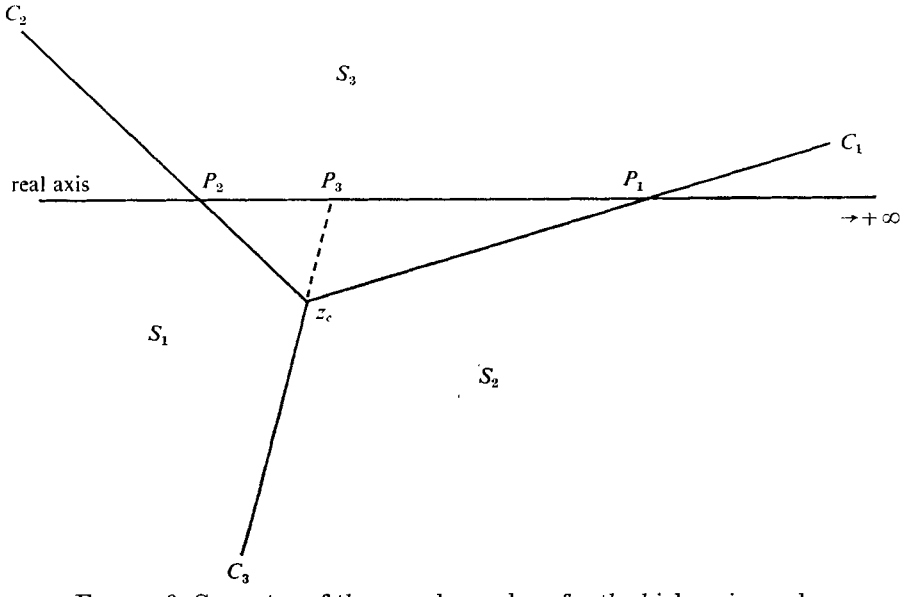

FIGURE 9. Geometry of the complex z plane for the higher eigenvalues of the Blasius boundary layer.

automatically satisfies the outer boundary conditions, but in Lin's solution the boundary conditions at $z = 0$ were satisfied only for the sum of the viscous and inviscid solutions. Equation (9) was therefore computed only outwards from z_c, with the results shown in figure 8. The close similarity between this graph and the corresponding curves in figure 5(*b*) confirms the predominantly viscous character of state 2.

Comparison with analytical theory

Our numerical solutions are not inconsistent with the analytical results established by Wasow (1948, 1950, 1953) and summarized by Lin (1955). Wasow proved that there exists a 'complete fundamental system' of functions of the complex variable z which provides solutions to the Orr–Sommerfeld equation in 'the full complex neighbourhood' of the branch point z_c. A comparison between our results and this analytical theory is of special interest because it suggests an explanation of the 'pairing' of the higher states.

For the damped solutions with which we are concerned, the analytical features of the complex z plane are illustrated in figure 9. z_c has a positive real part and a negative imaginary part. Three branch lines C_1, C_2 and C_3 representing the loci

$$\mathrm{Re}\int_{z_c}^{z} [i\alpha R\{U(z)-c\}]^{\frac{1}{2}}\,dz = 0$$

emerge from z_c at angles of $\frac{1}{6}\pi - \frac{1}{3}\arg\alpha$, $\frac{5}{6}\pi - \frac{1}{3}\arg\alpha$ and $\frac{3}{2}\pi - \frac{1}{3}\arg\alpha$. The function $U(z)$ is nearly linear for small values of z, and for our z_c values the branch lines are almost straight. C_1 and C_2 therefore intersect the real axis at P_1 and P_2. Wasow's proofs are given for a closed domain S defined by a bounding circle

centred on z_c and having a large but finite radius. Closed subdomains S_n are defined by the bounding circle and the lines $C_j, j \neq n$. The position of the origin of z in figure 9 depends on $\arg z_c$. For the fundamental and the higher eigenstates of even order it lies in S_1 slightly to the left of P_2, and for the eigenstates of odd order it lies in S_3 slightly to the right of P_2. The analytical solution differs in these two cases because the eigenfunctions extend in the first case into three subdomains and in the second case into only two.

Wasow's solution employs the seven functions A_n, U_n and V ($n = 1, 2, 3$), all of which are single valued and uniformly continuous in the following domains: A_n in $S - C_n$, U_n in $S - S_n$ and V in S. The functions A_n are viscous solutions, tending asymptotically to (8) as αR increases, the real part of the exponent being negative in S_n and positive in the adjacent subdomains. A_n is therefore discontinuous across C_n. The functions U_n are the asymptotically inviscid solutions, having a logarithmic singularity at z_c and Stokes-effect changes of form on crossing C_j, $j \neq n$. At finite values of αR the Orr–Sommerfeld equation is not singular; the singularities in A_n and U_n appear when analytical methods are used to separate the four independent functions which provide a complete analytical solution. Wasow gives three auxiliary relations connecting the seven functions, and these relations explain the continuity of the total solution in the neighbourhood of the branch lines; they also show that, in S_n, U_n assumes the character of the viscous solutions with positive real part for the exponent. Solutions of the Orr–Sommerfeld equation therefore exist on the real axis both when two subdomains and when three subdomains are involved.

When the origin of z lies in S_3, and the boundary conditions for $\phi(z)$ limit z to the sectors S_3 and S_2, the solution is of the form

$$\phi = V + U_1 + A_2. \tag{10a}$$

A_2 has an exponent with positive real part in S_3 and negative real part in S_2. When the origin lies in S_1, and the boundary conditions require z to extend from S_1 through S_3 to S_2, the solution is of the form

$$\phi = V + U_3 + A_2. \tag{10b}$$

Within S_3, U_3 behaves asymptotically like $A_1 + U_2$, and in this sector both A_1 and A_2 have exponents with positive real part.

The following comparison between the analytical and the numerical results is based on the seven eigenvectors computed with $R = 5000$ and $10^6 F = 80$. In every case, ϕ shows rapid oscillations attributable to the A_n functions. These occupy a range of z which decreases as the order of the state decreases, i.e. as the distance of z_c from the real axis decreases. The maximum amplitude of the oscillations occurs slightly outside P_3. The oscillations of the highest-order state (the eighth) remain detectable for a considerable distance within S_2. The A_n oscillations are superposed on slow variations in ϕ arising from V and U_n (see figures 5*b*, *c*); very weak fluctuations with wavelengths in the z direction of the order of the total boundary-layer thickness appear to arise from $V + U_n$. There is one marked difference between the numerical solutions for the odd and even orders. From the plate surface the phase angle of ϕ decreases monotonically for

the odd orders. For the even orders $\arg\phi$ increases until C_2 is crossed and then, changing steeply at first, decreases monotonically.

The eigenvalue thresholds and aggregate properties

The threshold eigenvalues of the higher states cannot be found directly, but the threshold condition $\gamma_r = 0$ is equivalent to $R(\alpha_r - \beta) = -2\alpha_r\alpha_i$, which makes α_r very slightly less than β. The remaining equation, $\gamma_i^2 = R\alpha_i - (\alpha_r^2 - \alpha_i^2)$, leaves the threshold values of γ_i and α_i indeterminate. Figure 7 suggests, however, that the $2n$ and $2n+1$ states have a common threshold with two-fold degeneracy, and that the thresholds for all the states lie near the line $\log\alpha_i = \log\alpha_r$. Since the intersections of the straight lines in figure 7 lie below this line, it is possible that α_i is slightly smaller than α_r at threshold. It may be noted here that the time-amplification eigenvalues were reported by Morawetz to have at most two-fold degeneracy.

Certain regularities in the distances between points in figure 7 were noted in §4, and these may be expressed by equations. If R and F have high values, so that many eigenvalues exist, and if $\alpha^{(n)}$ denotes the nth-order eigenvalue, then

$$\left.\begin{aligned} k_1\alpha_r^{(2)} &= k_n n\alpha_r^{(2n)} \sim k_n n\alpha_i^{(2n+1)} \\ l_1\alpha_i^{(2)} &= l_n n\alpha_i^{(2n)} \sim l_n n\alpha_r^{(2n+1)} \end{aligned}\right\} \quad \text{at constant } R \text{ and } F, \quad n = 2, 3, 4, \ldots,$$

where k_1 is about 0·8, the other k_n are constants rising to 1 as n increases, and l_1 and l_n behave like k_1^{-1} and k_n^{-1}. Thus k_n and l_n tend to unity as the range in z of the oscillatory part of ϕ increases. No simple connexion appears to exist between the equations given above and those given by Morawetz (see §1) for the viscous eigenvalues in time-amplified flows between parallel walls.

Other useful approximate relations that hold well above threshold are

$$\alpha_r^{(2)} \sim \begin{cases} \beta^{\frac{3}{2}} \text{ or } F^{\frac{3}{2}} & \text{at constant } R, \\ R^{\frac{1}{2}} & \text{at constant } \beta, \\ R^2 & \text{at constant } F. \end{cases}$$

The higher eigenstates for the perturbed boundary layer are all quite highly damped, and it follows that the 'group velocity' concept is not applicable to them (see, for example, Jeffreys & Jeffreys 1966; Brillouin 1946). The energy required to maintain the states must therefore be supplied from an external source. When this occurs, the eigenstates will have an 'energy velocity' governed by the velocity of propagation of the disturbance that supplies the energy.

The coupling of the mean flow and the boundary layer

This study has shown that the boundary layer possesses, in addition to the fundamental eigenstate, two series of higher eigenstates, each higher state having a threshold depending on R and F. On its first appearance each higher eigenvector has a low logarithmic decrement per wavelength in the z direction. The eigenvector then extends for a considerable distance into the inviscid region of the total flow. As R increases, the logarithmic decrement increases rapidly, and the oscillations become confined to the neighbourhood of z_c. This suggests

that the coupling of the boundary layer and the mean flow could be operated by eigenvectors having oscillations in the inviscid region.

The most important consequence of this coupling is the phenomenon of breakdown of laminar flow, which is well known to depend on the level of free-stream fluctuations. The finer details of breakdown under conditions of both natural and forced transition can be seen in the continuous recordings of hot-wire signals obtained by Schubauer & Klebanoff (1955) and Schubauer (1958). We are here interested mainly in their observations of natural transition. When the free-stream turbulence in their tunnel was reduced to 0·03 %, natural transition was preceded by the appearance of waves with a frequency of about 180 Hz, and it must be inferred that this frequency was prominent in the residual turbulence. One of the hot wires was mounted close to the flat plate, and its recordings show the following features of the breakdown process.

(i) The suddenness of the change in the boundary-layer flow. The breakdown process occupied a total time of the order of 0·003 s.

(ii) Within this short period there first appeared a few high frequency oscillations without change in the mean flow.

(iii) This was followed by an abrupt rise in mean velocity with superposed fluctuations indicating that turbulent-spot behaviour had supervened.

It is possible that these effects might be produced by a higher eigenstate which, at the effective local Reynolds number, crosses its threshold and thus becomes able, quite suddenly, to penetrate into the boundary layer. If the resulting disturbance of the previously established flow generated a Reynolds stress acting preferentially towards the plate surface, the fluid could be moved towards the plate surface to produce a rise in mean velocity and initiate turbulent-spot behaviour. In figure 1 of Schubauer & Klebanoff the beginning of natural transition occurs with $U_0 = 80$ ft/s, $X = 5{\cdot}6$ ft and a frequency of 180 Hz. These values give $R \sim 2820$ and $F \sim 29 \times 10^{-6}$, corresponding closely to the threshold for state 4, as shown in our table 2. It is not possible to give a similar comparison for breakdown in the calmed regions because the effective Reynolds number in these regions is not known.

The same authors show that, in the amplifying region, forced transition is more complicated than natural transition, involving an incipient breakdown stage which has been studied in greater detail by Klebanoff, Tidstrom & Sargent (1962) and Kovasznay, Komoda & Vasudeva (1962). All the recordings of incipient breakdown show the presence of nearly periodic, high frequency fluctuations superposed on the primary perturbation: fluctuations that are damped out rapidly within each primary cycle. This indicates the existence of a mechanism operating with perfect regularity and having a spatial periodicity which might be related to higher eigenstates.

The authors gratefully acknowledge the support of this work by the Department of Trade and Industry in meeting half the costs of computation and providing a maintenance grant for one of the authors (D.J.R.H.). A Science Research Council Studentship was awarded to D.C.

Appendix

By M. A. S. Ross

It has been suggested by a referee that a comparison should be made between our use of (6) and the methods developed by Bouthier (1972, 1973) and Gaster (1974) for solving the space-amplification stability problem in Blasius flow. These authors use stream functions in the form of series expansions in powers of the reciprocal of a boundary-layer Reynolds number; they introduce the downstream co-ordinate explicitly in the eigenfunction; they solve the Orr–Sommerfeld equation completely to find a first approximation to the eigenvalue, but they do not solve for the eigenfunction at their more accurate level of solution.

Gaster takes

$$\psi(\xi,\eta,t) = \{A(\xi)\,\phi_0(\xi,\eta) + R^{-\frac{1}{2}}\phi_1(\xi,\eta) + O(R^{-1})\}\,e^{Q}, \tag{A 1}$$

with $$Q = i\left\{R^{\frac{1}{2}}\int_1^{\xi}\frac{\alpha(\xi)}{\xi^{\frac{1}{2}}}d\xi - \beta t\right\}, \quad \xi = \frac{x}{x_0}, \quad \eta = y\left(\frac{U_0}{\nu x}\right)^{\frac{1}{2}}, \quad R = U_0 x_0/\nu.$$

Bouthier's (1972) equation (70) applied to the space-amplification case becomes

$$\psi(\xi,\eta,t) = \left\{A(\xi)\,\phi_0(\eta,\xi) + \frac{1}{\xi}\phi_1(\eta,\xi) + \frac{1}{\xi^2}\ldots\right\}\exp\left[i\lambda(\xi,t)\right], \tag{A 2}$$

with $$x + iy = (\nu/U_0)\,(\xi + i\eta)^2$$

and $$\xi = (U_0 x/\nu)^{\frac{1}{2}} \quad \text{for} \quad \eta \ll \xi.$$

Since

$$A(\xi) = \exp i\left[-i\int\frac{d}{d\xi}\log A(\xi)\,d\xi\right],$$

the function $(-i/A(\xi))\,dA(\xi)/d\xi$ is an additive correction to the wavenumber already present in the exponential factor in the stream function. The stability equations resulting from the introduction of (A 1) and (A 2) contain the Orr–Sommerfeld terms in ϕ_0, second-order terms in ϕ_0 and the highest-order terms in ϕ_1. After one stage of analytical integration with respect to η, the terms in ϕ_1 are eliminated and an ordinary differential equation for $A(\xi)$ remains.

To compare our method with the work of Bouthier and Gaster let us take a stream function in dimensional rectangular co-ordinates similar to the first term of (A 1) and (A 2), but with the possible amplitude factor $A(x)$ already absorbed in the exponent:

$$\psi(x,z,t) = \phi(x,z)\exp i\left[\int_{x_0}^{x}\alpha(x)\,dx - \beta t\right].$$

The real and imaginary parts of α differ greatly in their x dependence; for a sustained periodic disturbance, $\alpha_r(x)$ is nearly independent of x, while $\alpha_i(x)$ passes through a minimum which may have a positive (stable) or negative (unstable) value; moreover, at the peak of the neutral-stability curve, $\alpha_i = 0$

and $d\alpha_i/dx = 0$, and at this point the higher derivatives of α_i may be important. The main variations of ϕ are z dependent,

$$\frac{\partial\phi}{\partial x}\Big/\frac{\partial\phi}{\partial z} = O(R_x^{-\frac{1}{2}}),$$

and within the accuracy of the Blasius solution for the mean flow $\partial^2\phi/\partial x^2$ is negligible. The complete stability equation is then

$$\begin{aligned}(Ui\alpha - i\beta)(\phi'' - \alpha^2\phi) - U''i\alpha\phi - \nu(\phi^{\mathrm{iv}} - 2\alpha^2\phi'' + \alpha^4\phi) + W(\phi''' - \alpha^2\phi') - W''\phi' \\ + \left[2\alpha\beta - 3\alpha^2 U - U'' + U\frac{\partial^2}{\partial z^2} + 3iU\frac{d\alpha}{dx}\right]\frac{\partial\phi}{\partial x} + \left[\beta\frac{d\alpha}{dx} - 3\alpha\frac{d\alpha}{dx}U + i\frac{d^2\alpha}{dx^2}U\right]\phi \\ + i\frac{d\alpha}{dx}W\phi' + \nu\left[4i\alpha\frac{\partial^2}{\partial z^2} - 4i\alpha^3 - 12\alpha\frac{d\alpha}{dx} + 4i\frac{d^2\alpha}{dx^2}\right]\frac{\partial\phi}{\partial x} \\ + \nu\left[2i\frac{d\alpha}{dx}\frac{\partial^2}{\partial z^2} + i\frac{d^3\alpha}{dx^3} - 3\left(\frac{d\alpha}{dx}\right)^2 - 6i\alpha^2\frac{d\alpha}{dx} - 4\alpha\frac{d^2\alpha}{dx^2}\right]\phi = 0. \quad \text{(A 3)}\end{aligned}$$

In the immediate vicinity of the plate, where U and U'' are very small, the Orr–Sommerfeld equation reduces to

$$-i\beta(\phi'' - \alpha^2\phi) - \nu(\phi'''' - 2\alpha^2\phi'') \sim 0.$$

The absolute magnitude of these two terms near the plate can greatly exceed the magnitude of any other term at any larger z. It follows that near the plate a significant second-order effect may come from the viscous term.

In our method the solution of (A 3) is found in very long and thin strip elements, each extending in the z direction from the plate into the free stream and having in the x direction a width dx sufficient to accommodate only first-order x derivatives. It is necessary to decide which terms of (A 3) will be significant within the elementary strip.

Consider first the integral

$$\int_{x_0}^{x} \alpha(x)\,dx.$$

This integral is meaningful only when it is taken over a range of x within which α is variable. In our strip of infinitesimal width, α can be treated as a local constant, and the integral becomes $\alpha(x)\,dx$. It is clear that for our method the exponent in (2) is preferable to the form assumed here. The x in (2) must, however, be regarded as having an arbitrary origin, while the x required to calculate U, W or R has origin at the leading edge of the plate. All the x derivatives of α will be omitted from (A 3). This does not mean that the x derivatives of α cannot be found, but merely that to find them two or more strips at different values of x must be used. The derivatives will all be present in the solution taken over a sufficient range of x.

The equation has now been reduced to the first line of (A 3) and six terms involving $\partial\phi/\partial x$, four in line 2 and two in line 3. With the strip centred at a chosen value of x, the dimensional values of U, U'', W and W'' are calculated. These functions may be assumed to be constant over the width of the strip, and

thus to be functions of z alone. This assumption is *not* equivalent to assuming the mean flow to be parallel to the plate; the direction of the mean flow is z dependent. Since all the coefficients of the remaining terms in (A 3) are either constant or z dependent, the equation is separable in x and z. Writing $\phi(x,z) = C(x)F(z)$ and taking L_A and L_B as the operators generating the terms multiplied respectively by $C(x)$ and $dC(x)/dx$, we have

$$\frac{L_A[F(z)]}{L_B[F(z)]} = -\frac{1}{C(x)}\frac{dC(x)}{dx} = -ik,$$

where k is a constant of order $R_x^{-\frac{1}{2}}$ (with negligible second and higher powers) which cannot be determined for lack of boundary conditions in x. Also

$$L_A[F(z)] + ikL_B[F(z)]$$

for wavenumber α is $L_A[F(z)]$ for wavenumber $\alpha + k$. Thus k appears to be an uncertainty of order $R_x^{-\frac{1}{2}}$ in the wavenumber. The six remaining terms in lines 2 and 3 of (A 3) have now become absorbed in terms in the first line, reducing (A 3) to the dimensional form of (6).

It is necessary to ask whether the resulting solution for α is indeed subject to an uncertainty introduced by k. In our view the answer is no. The uncertainty arises because x has been introduced explicitly in ϕ. If this is not done then ϕ is still x dependent: in the dimensional equation through downstream changes in U and W and in the dimensionless case through R and the dimensionless $Z = z/\delta_1 = z/sx^{\frac{1}{2}}$, with $s = 1{\cdot}7208(U_0/\nu)^{\frac{1}{2}}$. The introduction of x explicitly in ϕ is redundant for our method of solution.

Since a non-dimensional solution is required, the reduced form of (A 3) is made non-dimensional using the local value of δ_1 as the unit of length. Numerical solution of (6) by the method of Ross & Corner (1972) gives simultaneously the eigenfunction and eigenvalue as functions of $R = U_0\delta_1/\nu$.

Let us now consider the question of the continuity of solutions obtained by strip integration, doubts about which appear to have led to the investigations of Bouthier and Gaster. It was realized by Schubauer & Skramstad (1947) that the amplification should be expressed in dimensional variables. The dimensional continuity equation and stream function are applicable at all x. The dimensionless solution

$$\psi = F(Z)\exp i(\alpha' X - \beta t),$$

with $Z = z/sx^{\frac{1}{2}}$, $X = x^{\frac{1}{2}}/s$ and $\alpha' = \alpha s x^{\frac{1}{2}}$, converts to

$$\psi = U_0 s x^{\frac{1}{2}} F(z/sx^{\frac{1}{2}})\exp i(\alpha x - \beta t),$$

giving

$$u = \partial\psi/\partial z = U_0 F'(z/sx^{\frac{1}{2}})\exp i(\alpha x - \beta t)$$

and

$$\frac{1}{u}\frac{\partial u}{\partial x} = i\alpha + \frac{1}{F'}\frac{\partial F'}{\partial x} \quad \text{with} \quad F' = \frac{\partial F}{\partial Z}. \tag{A 4}$$

The real part of (A 4) gives the amplification constant. The term $i\alpha$ carries the amplification within a strip and the second term carries the more complicated x- and z-dependent change on passing through a succession of contiguous strips.

The conclusion drawn from the above arguments is that (6) is a correct and complete equation for the solution of the Blasius stability problem. A complete eigenstate solution is obtainable, and the arbitrary numerical factor introduced in the normalization of $F(z)$ cancels out in the complete expression for the amplification constant.

REFERENCES

BARRY, M. D. J. & ROSS, M. A. S. 1970 *J. Fluid Mech.* **43**, 813.

BOUTHIER, M. 1972 *J. Méc.* **11**, 599.

BOUTHIER, M. 1973 *J. Méc.* **12**, 75.

BRILLOUIN, L. 1946 *Wave Propagation in Periodic Structures*, chap. 5. McGraw-Hill.

GASTER, M. 1974 *J. Fluid Mech.* **66**, 465.

JEFFREYS, H. & JEFFREYS, B. S. 1966 *Methods of Mathematical Physics*, pp. 511–515. Cambridge University Press.

JORDINSON, R. 1971 *Phys. Fluids*, **14**, 2535.

KLEBANOFF, P. S., TIDSTROM, K. D. & SARGENT, L. M. 1962 *J. Fluid Mech.* **12**, 1.

KOVASZNAY, L. S. G., KOMODA, H. & VASUDEVA, B. R. 1962 *Proc. Heat Transfer Fluid Mech. Inst.*, p. 1. Stanford University Press.

LIN, C. C. 1944 *Quart. Appl. Math.* **3**, 117, §4(*b*).

LIN, C. C. 1955 *The Theory of Hydrodynamic Stability*, chap. 8. Cambridge University Press.

MACK, L. M. 1976 *J. Fluid Mech.* **73**, 497.

MORAWETZ, C. S. 1952 *J. Rat. Mech. Anal.* **1**, 579.

ROSS, M. A. S. & CORNER, D. F. 1972 *Proc. Roy. Soc. Edin.* **70**, 251.

SCHENSTED, I. V. 1961 Contributions to the theory of hydrodynamic stability. Ph.D. thesis, University of Michigan.

SCHUBAUER, G. B. 1958 In *Proc. Symp. Boundary Layer Res., Int. Un. Theoret. Appl. Mech., Freiburg*, p. 85.

SCHUBAUER, G. B. & KLEBANOFF, P. S. 1955 *Nat. Advis. Comm. Aero. Wash. Rep.* no. 1289.

SCHUBAUER, G. B. & SKRAMSTAD, H. K. 1947 *J. Res. Nat. Bur. Stand.* **38**, 251.

WASOW, W. 1948 *Ann. Math.* **49**, 852.

WASOW, W. 1950 *Ann. Math.* **52**, 350.

WASOW, W. 1953 *Ann. Math.* **58**, 222.